SUPPLEMENTARY INFORMATION

Tuning the metal-insulator transition in $NdNiO_3$ heterostructures via Fermi surface instability and spin-fluctuations

R. S. Dhaka*
Swiss Light Source, Paul Scherrer Institute, CH-5232 Villigen PSI, Switzerland
Institute of Condensed Matter Physics, Ecole Polytechnique Fédérale de Lausanne (EPFL), CH-1015 Lausanne, Switzerland and
Department of Physics, Indian Institute of Technology Delhi, Hauz Khas, New Delhi-110016, India

Tanmoy Das
Department of Physics, Indian Institute of Science, Bangalore-560012, India and
Department of Physics, National University of Singapore, Singapore

N. C. Plumb, N. Xu, and M. Shi
Swiss Light Source, Paul Scherrer Institute, CH-5232 Villigen PSI, Switzerland

Z. Ristic
Swiss Light Source, Paul Scherrer Institute, CH-5232 Villigen PSI, Switzerland and
Institute of Condensed Matter Physics, Ecole Polytechnique Fédérale de Lausanne (EPFL), CH-1015 Lausanne, Switzerland

W. Kong
Swiss Light Source, Paul Scherrer Institute, CH-5232 Villigen PSI, Switzerland and
Institute of Physics, Chinese Academy of Sciences, Beijing 100190, China

C. E. Matt
Swiss Light Source, Paul Scherrer Institute, CH-5232 Villigen PSI, Switzerland and
Laboratory for Solid State Physics, ETH Zürich, CH-8093 Zürich, Switzerland

Kapildeb Dolui
Department of Physics, National University of Singapore, Singapore

E. Razzoli
Department of Physics, University of Fribourg, CH-1700 Fribourg, Switzerland

M. Medarde
Laboratory for Developments and Methods, Paul Scherrer Institut, CH-5232 Villigen PSI, Switzerland

L. Patthey
SwissFEL, Paul Scherrer Institute, CH-5232 Villigen PSI, Switzerland

M. Radović†
Swiss Light Source, Paul Scherrer Institute, CH-5232 Villigen PSI, Switzerland and
SwissFEL, Paul Scherrer Institute, CH-5232 Villigen PSI, Switzerland

Joël Mesot‡
Swiss Light Source, Paul Scherrer Institute, CH-5232 Villigen PSI, Switzerland
Institute of Condensed Matter Physics, Ecole Polytechnique Fédérale de Lausanne (EPFL), CH-1015 Lausanne, Switzerland and
Laboratory for Solid State Physics, ETH Zürich, CH-8093 Zürich, Switzerland

(Dated: May 7, 2015)

* rsdhaka@physics.iitd.ac.in
† milan.radovic@psi.ch
‡ joel.mesot@psi.ch

DFT calculations

Earlier calculations in the heterostructure of $LaNiO_3$ and $LaAlO_3$ show that its electronic structure is very much same as the bulk $LaNiO_3$ apart from tiny reduction of three-dimensionality [1]. Following the same strategy of Ref. [2], we carry out the density functional calculation of NNO using the Vienna *ab-initio* simulation package [3] within the GGA+U of PBE parametrization [4]. Projected augmented-wave (PAW) [5, 6] pseudo-potentials are used to describe core electrons. We use $U = 3.5$ eV, which is larger than the values of U used in the self-energy calculation. This is expected since the bare U used in the self-energy calculation is further multiplied by various components of the susceptibility to provide the effective many-body potential in this calculation, as described below. Bulk $NdNiO_3$ belongs to the P4/mmm space group and a A type antiferromagnetic spin ordering [2] is imposed in the system to obtain a stable ground state [2]. The electronic wave-function is expanded using plane waves up to a cutoff energy of 500 eV. Brillouin zone sampling is done by using a (12×12×6) Monkhorst-Pack k-grid.

Tight binding fitting

To accurately compute the electron-electron correlation in this system, we derive the tight-binding Hamiltonian for the three lowest energy states. As evident from the DFT band structure, the low-energy states mainly composed of two e_g orbitals which constitute the electron and hole pockets, while a third hole pocket develops near 'A' point coming from the hybridized state of t_{2g} of Ni atoms with the p-orbitals of O atoms. To restrict our methodology within the essential three bands model, we model the third band as an effective state of all these orbitals. Therefore, in the three band tight-binding model, the non-interacting Hamiltonian can be written as

$$\tilde{H} = \hat{\Psi}^\dagger \begin{pmatrix} \xi_{1,\mathbf{k}} & \xi_{12,\mathbf{k}} & \xi_{13,\mathbf{k}} \\ & \xi_{2,\mathbf{k}} & \xi_{23,\mathbf{k}} \\ h.c. & & \xi_{3,\mathbf{k}} \end{pmatrix} \hat{\Psi}. \tag{1}$$

The symbol tilde over a quantity in this paper denotes it to be a matrix. Here the non-interacting dispersions for intra- and inter-orbital hoppings are derived by considering the three-dimensional crystal symmetry of the tetragonal lattice. If we define $\xi_{1,\mathbf{k}}$, $\xi_{2,\mathbf{k}}$ and $\xi_{3,\mathbf{k}}$ as dispersion for $d_{x^2-y^2}$, d_{z^2}, and effective d_{xy} orbitals, respectively, we obtain

$$\begin{aligned} \xi_{1,\mathbf{k}} &= -2t_1(c_x + c_y) - 4t_2 c_x c_y + \delta_1 - \mu, \\ \xi_{2,\mathbf{k}} &= -2t_3(c_x + c_y) - 4t_4 c_x c_y - 2t_5 c_z + \delta_2 - \mu, \\ \xi_{3,\mathbf{k}} &= -2t_6(c_x + c_y) - 2t_7 c_z + \delta_3 - \mu, \end{aligned} \tag{2}$$

and,

$$\begin{aligned} \xi_{12,\mathbf{k}} &= -2t_8(c_x - c_y), \\ \xi_{13,\mathbf{k}} &= -2t_9(c_x + c_y), \\ \xi_{23,\mathbf{k}} &= -2t_{10} c_x c_y. \end{aligned} \tag{3}$$

Here $c_i = \cos k_i$ for $i = x, y, z$. t_i are various nearest and next-nearest neighbor hoppings, δ_i are the onsite potentials for different orbitals, and μ is the system's chemical potential. The corresponding tight-binding parameters are obtained by fitting the eigenvalues of the above Hamiltonian to the corresponding DFT band structure as shown in Fig. S1. Hence we obtain t_1=0.41, t_2=-0.12, δ_1=0, t_3=0.05, t_4=0.04, t_5=0.35, δ_2=-0.1, t_6=0.23, t_7=0.15, δ_3=-1.8, t_8=0.2, t_9=0.1, t_{10}=0.1, all in eV. All the parameters remain same for the case of NNO/LAO, except the onsite term for the d_{xy} is reduced to -1.5 eV, and the hopping between d_{xy} to the two e_g orbitals is reduced to 0.15 eV. The chemical potential is estimated for each samples to keep the number of electrons same after including the self-energy effects. After projecting the orbital character on the corresponding band structure, we find that the dominant orbital contribution to both electron and hole pockets comes from the $d_{x^2-y^2}$ orbital as in cuprats (without the electron pocket). The corresponding Fermi surface is shown in the paper, see Fig. 6(h). For NNO/LAO case, the electron-pocket becomes smaller while the hole pocket increases, and an additional hole-pocket appears around the 'A' point, see Fig. 6(i) of the paper.

More details of the MRDF method

The transition metal oxides reside in the metal-insulator boundary which indicates that the strength of the Coulomb interaction is neither sufficiently large to localize all electrons, nor weak enough to define a quasiparticle peak at all energy and momenta. In this spirit it is appropriate to apply an intermediate coupling theory, [9–11] which allows the coexistence of itinerant and localized electrons in different momentum and energy regions of the spectra.

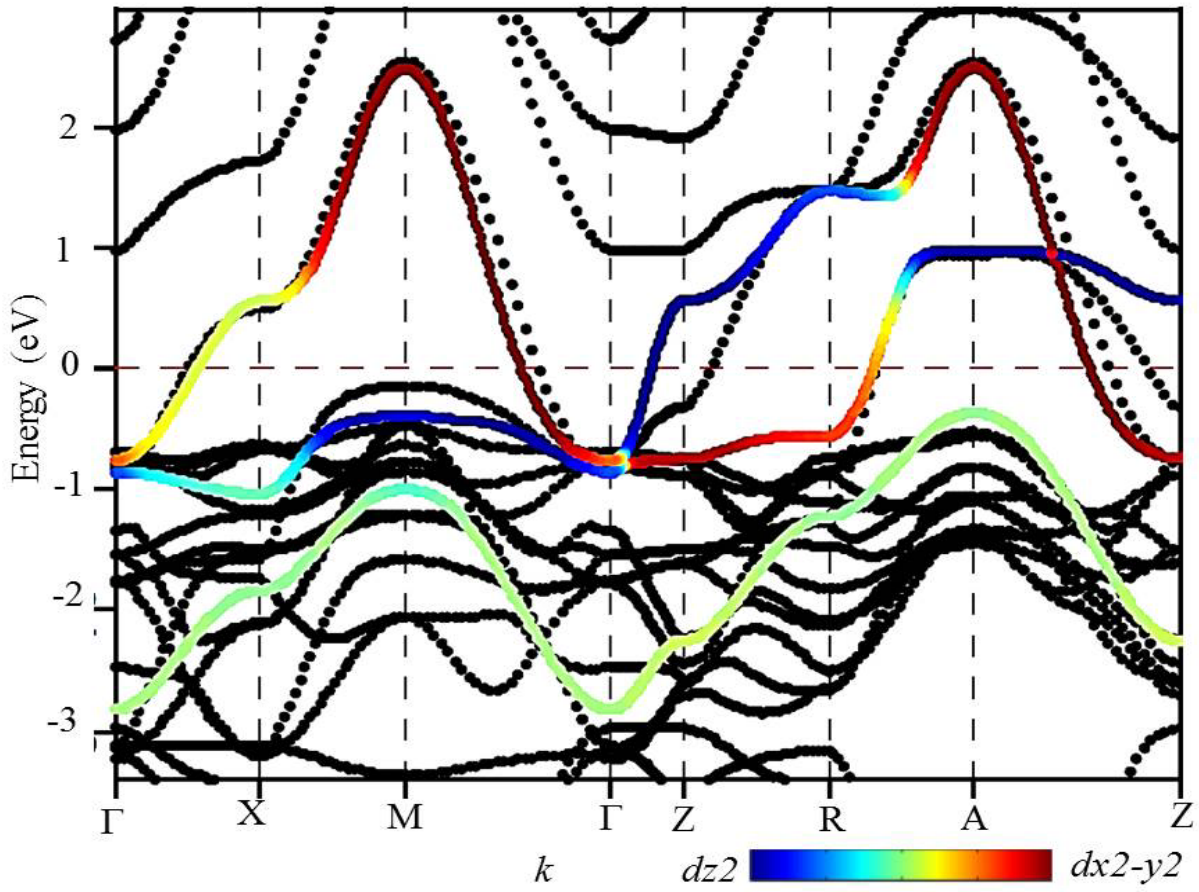

FIG. 1. DFT band structure for NNO. Superimposed are the tight-binding bands calculated from the Hamiltonian in Eq. (1). The color coating of the tight-binding line gives the relative weight of d_{z^2} (blue) to $d_{x^2-y^2}$ (red) orbital character while light green color gives the weight of the hybridized d_{xy}-orbital.

The single-particle Green's function is defined as $\tilde{G}_0(\mathbf{k}, i\omega_n) = \left(i\omega_n \tilde{1} - \tilde{H}\right)^{-1}$, where $i\omega_n$ is the Matsubara frequency for the fermions, and H is the non-interacting tight-binding Hamiltonian. The explicit form of G is then obtained as

$$G_{mn}(\mathbf{k}, i\omega_n) = \sum_{\nu} \frac{\phi^{\nu}_{\mathbf{k},m} \phi^{\nu\dagger}_{\mathbf{k},n}}{i\omega_n - \xi^{\nu}_{\mathbf{k}}}. \tag{4}$$

Here $\mathbf{k}$ and ω are the quasiparticle momentum and frequency, and $\mathbf{q}$ and ω_p are the bosonic excitation momentum and frequency, respectively. $\phi^{\nu}_{\mathbf{k},m}$ is the eigenstate for the ν^{th} tight-binding band ($\xi^{\nu}_{\mathbf{k}}$), projected onto the m^{th} orbital. The non-interacting density fluctuation susceptibility is

$$\chi^{st}_{0,mn}(\mathbf{q}, \omega_p) = -\frac{1}{\Omega_{\text{BZ}}\beta} \sum_{\mathbf{k},n} G_{mn}(\mathbf{k}, i\omega_n) G_{st}(\mathbf{k}+\mathbf{q}, i\omega_n + \omega_p), \tag{5}$$

where $\beta = 1/k_B T$, and k_B is the Boltzmann constant and T is temperature. Ω_{BZ} is the electronic phase space volume. $f^{\nu}_{\mathbf{k}}$ and n_p are the fermion and boson occupation numbers, respectively. After performing the Matsubara summation over the fermionic frequency ω_n and taking analytical continuation to the real frequency as $\omega_n \to \omega + i\delta$, we get

$$\chi^{st}_{0,mn}(\mathbf{q}, \omega_p) = -\frac{1}{\Omega_{\text{BZ}}} \sum_{\mathbf{k},\nu,\nu'} \phi^{\nu\dagger}_{\mathbf{k}+\mathbf{q},s} \phi^{\nu}_{\mathbf{k}+\mathbf{q},t} \phi^{\nu'}_{\mathbf{k},n} \phi^{\nu'\dagger}_{\mathbf{k},m} \frac{f^{\nu}_{\mathbf{k}+\mathbf{q}} - f^{\nu'}_{\mathbf{k}}}{\omega_p + i\delta - \xi^{\nu'}_{\mathbf{k}} + \xi^{\nu}_{\mathbf{k}+\mathbf{q}}}. \tag{6}$$

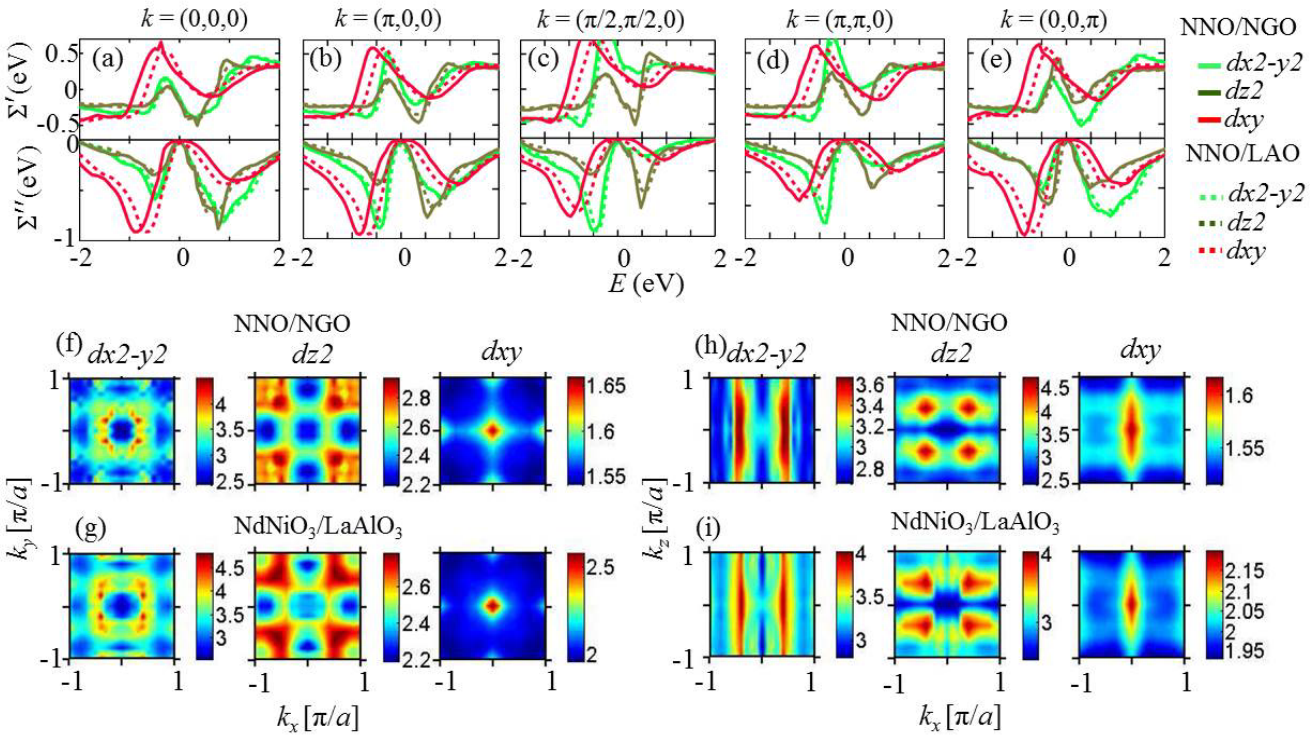

FIG. 2. Comparison of self-energy and band renormalization for NNO/NGO and NNO/LAO. For the same value of the interaction parameters, we find that the band renormalization and imaginary part of the self-energy are smaller in NNO/LAO than the other one.

The RPA Hamiltonian for the multiband system is

$$H_{\rm int} = \sum_{\mathbf{k}_1-\mathbf{k}_4}\Bigg[U\sum_m c^\dagger_{1,m\uparrow}c_{\mathbf{k}_2,m\uparrow}c^\dagger_{\mathbf{k}_3,m\downarrow}c_{k_4,m\downarrow} + \sum_{m<n,\sigma}\Big(Vc^\dagger_{\mathbf{k}_1,m\sigma}c_{\mathbf{k}_2,m\sigma}c^\dagger_{\mathbf{k}_3,n\bar\sigma}c_{\mathbf{k}_4,n\bar\sigma} + (V-J_H)c^\dagger_{\mathbf{k}_1,m\sigma}c_{\mathbf{k}_2,m\sigma}c^\dagger_{\mathbf{k}_3,n\sigma}c_{\mathbf{k}_4,n\sigma}\Big)$$
$$+ \sum_{m<n,\sigma}\Big(J_Hc^\dagger_{\mathbf{k}_1,m\sigma}c^\dagger_{\mathbf{k}_3,n\bar\sigma}c_{\mathbf{k}_2,m\bar\sigma}c_{\mathbf{k}_4,n\sigma} + J'c^\dagger_{\mathbf{k}_1,m\sigma}c^\dagger_{\mathbf{k}_3,m\bar\sigma}c_{\mathbf{k}_2,n\bar\sigma}c_{\mathbf{k}_4,n\sigma} + h.c.\Big)\Bigg]. \tag{7}$$

Here $c^\dagger_{\mathbf{k}_1,m\sigma}$ ($c_{\mathbf{k}_1,m\sigma}$) is the creation (annihilation) operator for an orbital m at crystal momentum $\mathbf{k}_1$ with spin $\sigma =\uparrow$ or $\downarrow$, where $\bar\sigma$ corresponds to opposite spin of σ. In the multiorbital spinor, the above interacting Hamiltonian can be collected in a interaction tensor $\tilde U_{s/c}$, where the subscripts s, c stand spin and charge density fluctuations. The nonzero components of the matrices $\tilde U_c$ and $\tilde U_s$ are given as

$$\tilde U^{mm}_{s,mm} = U, \quad \tilde U^{mm}_{s,nn} = \frac{1}{2}J_H, \quad \tilde U^{mn}_{s,mn} = \frac{1}{4}J_H + V, \quad \tilde U^{nm}_{s,mn} = J',$$
$$\tilde U^{mm}_{c,mm} = U, \quad \tilde U^{mm}_{c,nn} = 2V, \quad \tilde U^{mn}_{c,mn} = \frac{3}{4}J_H - V, \quad \tilde U^{nm}_{c,mn} = J'. \tag{8}$$

Of course, it is implicit that all the interaction parameters are orbital dependent. Within the RPA, spin and charge channels become decoupled. The collective many-body corrections of the density-fluctuation spectrum can be written in matrix representation: $\tilde\chi_{s/c} = \tilde\chi^0[\tilde 1 \mp \tilde U_{s/c}\tilde\chi^0]^{-1}$, for spin and charge densities, respectively. $\tilde\chi^0$ matrix consists of components $\chi^{st}_{0,mn}$ with the same basis in which the interactions $\tilde U_{s/c}$ are defined above.

Finally, the density fluctuation exchange potentials for the electronic state are computed as

$$V^{st}_{mn,i}(\mathbf{q},\omega_p) = \frac{\eta_i}{2}\left[\tilde U_i\tilde\chi''_i(\mathbf{q},\omega_p)\tilde U_i\right]^{st}_{mn}, \tag{9}$$

where i stands for spin and charge components, $\eta = 3$, 1 for the spin and charge channels, respectively. The feedback effect of the electronic interaction on the electronic spectrum is then calculated via self-energy calculation within the

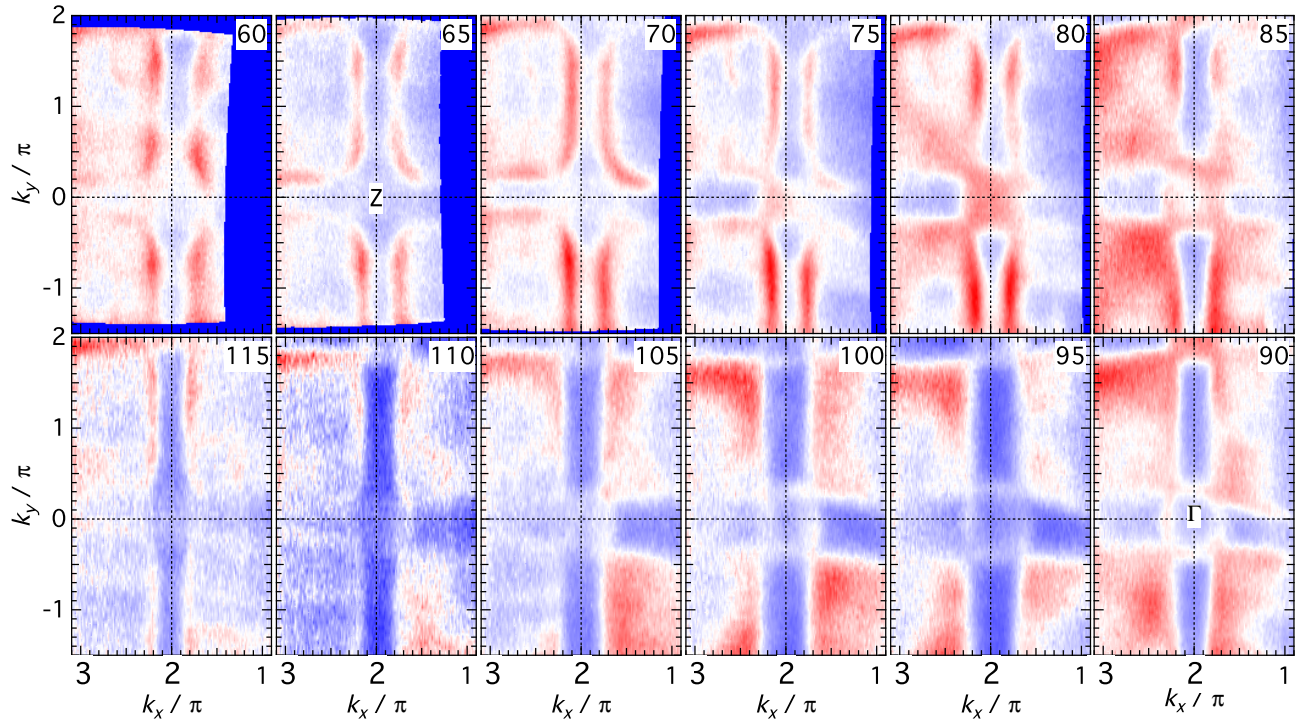

FIG. 3. The Fermi surface maps of 20 uc $NdNiO_3$ thin films grown on $NdGaO_3$, measured at 200 K sample temperature and as a function of photon energies ranging from 60 eV to 115 eV with 5 eV steps.

MRDF method[9–11]

$$\Sigma_{mn,i}(\mathbf{k},\omega) = \frac{1}{\Omega_{\rm BZ}} \sum_{\mathbf{q},st,\nu} \int_{-\infty}^{\infty} d\omega_p V^{st}_{mn,i}(\mathbf{q},\omega_p)\Gamma^{st}_{mn,\nu}(\mathbf{k},\mathbf{q}) \left[\frac{1-f^{\nu}_{\mathbf{k}-\mathbf{q}}+n_p}{\omega+i\delta-\xi^{\nu}_{\mathbf{k}-\mathbf{q}}-\omega_p} + \frac{f^{\nu}_{\mathbf{k}-\mathbf{q}}+n_p}{\omega+i\delta-\xi^{\nu}_{\mathbf{k}-\mathbf{q}}+\omega_p} \right], \quad (10)$$

where the subscript i stands for spin, charge and phonon contributions. The vertex correction $\Gamma^{st}_{mn,\nu}(\mathbf{k},\mathbf{q})$ encodes both the angular and dynamical parts of the vertex, which are combined to obtain $\Gamma^{st}_{mn,\nu}(\mathbf{k},\mathbf{q}) = \phi^{\nu\dagger}_{\mathbf{k}-\mathbf{q},s}\phi^{\nu}_{\mathbf{k}-\mathbf{q},t}(1 - \partial\Sigma_{mn}(\mathbf{k}-\mathbf{q},\omega)/\partial\omega)_0$. Full self-consistency requires the bare Green's function G_0 in Eq. (4) to be replaced with the self-energy dressed $\tilde{G}^{-1}(\mathbf{k},\omega) = \tilde{G}_0^{-1}(\mathbf{k},\omega) - \tilde{\Sigma}(\mathbf{k},\omega)$, where the total self-energy tensor is $\tilde{\Sigma}(\mathbf{k},\omega) = \tilde{\Sigma}_s(\mathbf{k},\omega) + \tilde{\Sigma}_c(\mathbf{k},\omega) + \tilde{\Sigma}_p(\mathbf{k},\omega)$,y and calculate susceptibilities and self-energies with the dressed Green's function until the self-energies converges. This procedure is numerically expensive, especially in the multiband systems and when full momentum dependence is retained. Therefore, we adopt a modified self-consistency scheme, where we expand the real part of the total self-energy tensor as $\tilde{\Sigma}'(\mathbf{k},\omega) = (1-\tilde{Z}_{\mathbf{k}})^{-1}\omega$ in the low-energy region [$|\omega| < 0.2-0.3$ eV in the present materials]. The resulting self-energy dressed quasiparticle dispersions $\bar{\xi}^{\nu}(\mathbf{k}) = Z^{\nu}_{\mathbf{k}}\xi^{\nu}(\mathbf{k})$ are used in Eqs. (4)-(10), which keep all the formalism unchanged with respect to the momentum resolved orbital selective quasiparticle renormalization factor $\tilde{Z}_{\mathbf{k}}$.

Origin of stronger correlation in NNO/NGO system:-

Eq. 10 indicates that the dominant contributions to the self-energy come from the large density of states (embedded in the Green's function G), and the susceptibilities term χ for a given set of the Coulomb interaction terms $\tilde{U}$. To effectively explain the origin of the large renormalization effect in NNO/NGO than NNO/LAO, we keep all the band parameters and the Coulomb interaction $\tilde{U}$ same in both systems, and change only the onsite potential by about 300 meV and the inter-orbital hoppings between e_g and t_{2g} orbitals. As seen from the band structure plot in Fig. S1, as we go from NNO/LAO to NNO/NGO, we approach toward the van-Hove singularity (VHS) of $d_{x^2-y^2}$ orbital on the $k_z = 0$ plane and of d_{z^2} orbital on the $k_z = \pi$ plane. That means the system approaches towards large density of states instability. A similar increment in the susceptibility is also visible for the NNO/NGO system. In this many-body case, the spin fluctuation is clearly more important than the charge counterparts. By comparing the integrated spin susceptibilities for the two systems, we see a considerable changes. In the low-energy region, we see that the

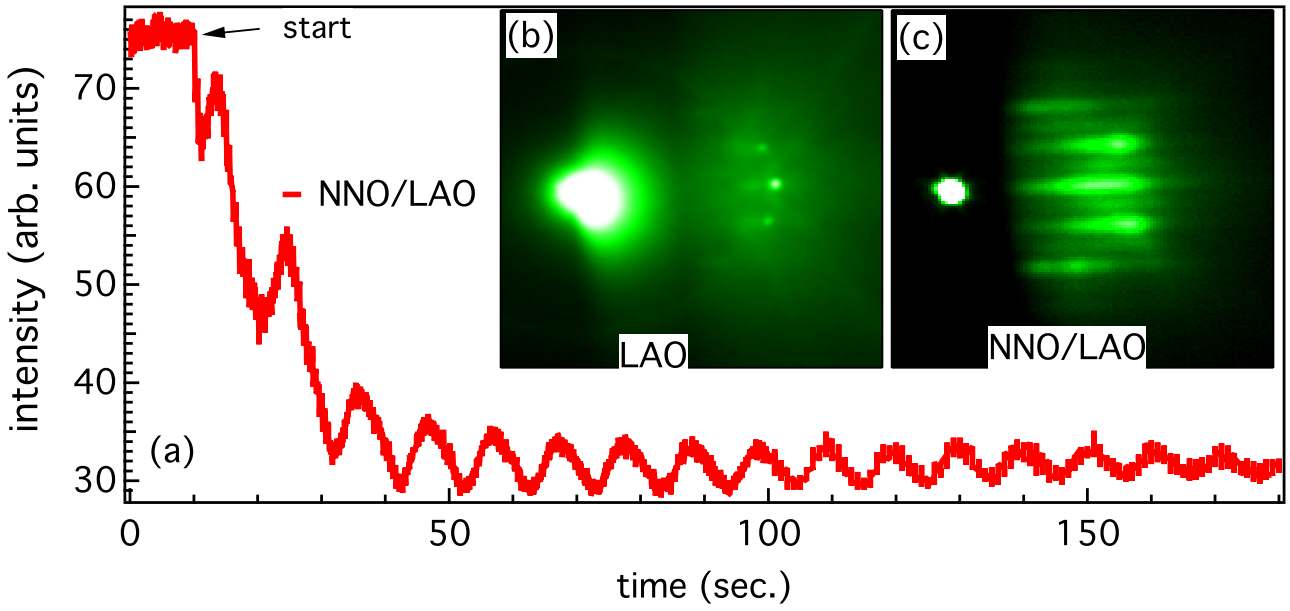

FIG. 4. (a) Typical RHEED intensity oscillations of NNO/LAO. (b,c) RHEED patterns of LAO substrate as well as NNO films grown on LAO substrate, respectively.

susceptibility is stronger in NNO/NGO, and concentrated around the wavevector $\mathbf{q} \sim (1/4, 1/4, 1/4 \pm \delta)$ instead of being spread out over a large momentum span as in NNO/LAO. This means NNO/NGO is prone to a magnetic instability. Similarly, the integrated spin susceptibility over the whole energy scale shows that while it is very much similar in the $k_z = 0$ plane, on the $k_z = \pi$ plane, it is larger for the NNO/NGO system. This result indicates that the dynamical fluctuation, and thus the renormalization effect is larger in NNO/NGO than in NNO/LAO.

This observation is also reflected in the numerical values of Σ and corresponding renormalization effect as shown in Fig. S2. In the top panels of Fig. S2, we show the same energy dependent self-energy for three orbitals and two systems at five representative high-symmetry momenta values. The general conclusion drawn at all these momenta by comparing the solid (NNO/NGO) and dashed (NNO/LAO) lines that the self-energies are larger in intensity for the NNO/NGO case, and the corresponding slope in Σ' (determining the strength of mass enhancement at the Fermi level) is also higher in this system. The overall k-profiles of the Z also reflect the same that the average renormalization increases in NNO/NGO than in NNO/LAO in all orbitals except in the d_{xy} one. This is because, the d_{xy} only crosses the Fermi level for the latter system which thereby obtain stronger renormalization effect.

Additional experimental details:-

In order to show the evolution of the electron and hole pockets, we present, in Fig. S3, the Fermi surface maps of 20 uc $NdNiO_3$ thin films grown on $NdGaO_3$, measured at 200 K sample temperature and as a function of photon energies ranging from 60 eV to 115 eV with 5 eV steps. In Fig. S4, we show typical RHEED oscillations during the growth of NNO thin films on LAO substrate. The corresponding RHEED patten is shown in Figs. S(b,c) for LAO substrate and NNO/LAO system, respectively, which show the well-ordered, high-quality single crystalline surface of the deposited thin films.

[1] Hansmann, P., Yang, X., Toschi, A., Khaliullin, G., Andersen, O. K., and Held, K. Turning a nickelate Fermi surface into a cupratelike one through heterostructuring. Phys. Rev. Lett. **103**, 016401 (2009).

[2] Liu, J., Kargarian, M., Kareev, M., Gray, B., Ryan, P. J., Cruz, A., Tahir, N., Chuang, Yi-De, Guo, J., Rondinelli, J. M., Freeland, J. W., Fiete, G. A. and Chakhalian, J. Heterointerface engineered electronic and magnetic phases of $NdNiO_3$ thin films. Nature Communications **4**, 2714 (2013).

[3] Kresse, G. and Furthmüller, J., Efficient iterative schemes for *ab-initio* total-energy calculations using a plane-wave basis set, Phys. Rev. B 54, 11169-11186 (1996).

[4] Perdew, John P. and Burke, Kieron and Ernzerhof, Matthias, Generalized Gradient Approximation Made Simple, Phys. Rev. Lett. **77**, 3865-3868 (1996)
[5] Kresse, G. and Joubert, D. From ultrasoft pseudopotentials to the projector augmented-wave method. Phys. Rev. B **59**, 1758 (1999).
[6] Blochl, P. E. Projector augmented-wave method. Phys. Rev. B **50**, 17953 (1994).
[7] Anisimov, V. I., Aryasetiawan, F. and Lichtenstein, A. I. First-principles calculations of the electronic structure and spectra of strongly correlated systems: the LDA–U method. J. Phys. Condens. Matter **9**, 767 (1997).
[8] Dudarev, S. L., Botton, G. A., Savrasov, S. Y., Humphreys, C. J. and Sutton, A. P. Electron-energy-loss spectra and the structural stability of nickel oxide: an LSDA–U study. Phys. Rev. B **57**, 1505 (1998).
[9] T. Das, R. S. Markiewicz, and A. Bansil, Intermediate coupling model of the cuprates, Adv. Phys. **63**, 151 (2014).
[10] T. Das, J. -X. Zhu, and M. J. Graf, Spin-fluctuations and the peak-dip-hump feature in the photoemission spectrum of actinides, Phys. Rev. Lett. **108**, 017001 (2012).
[11] T. Das, and K. Dolui, Superconducting dome in MoS2 and TiSe2 generated by quasiparticle-phonon coupling, Phys. Rev. B **91**, 094510 (2015).
[12] Kubo, K. Pairing symmetry in a two-orbital Hubbard model on a square lattice. Phys. Rev. B **75**, 224509 (2007).